RFI subtraction from time-averaged spectroscopy using a reference horn and cross power spectra

F. H. Briggs

Kapteyn Astronomical Institute, University of Groningen Postbus 800 9700 AV Groningen, The Netherlands; fbriggs@astro.rug.nl

J. F. Bell & M. J. Kesteven

CSIRO Australia Telescope National Facility, PO Box 76 Epping NSW 1710, Australia; jbell@atnf.csiro.au, mkesteve@atnf.csiro.au

ABSTRACT

Effective radio frequency interference (RFI) cancellation for spectroscopic applications can take place using time averaged spectra. An RFI "reference signal," constructed from the cross power spectrum of the signals from the two polarizations of a reference horn pointed at the source of the RFI signal, in combination with cross power spectra with the signals from the Parkes telescope, allows computation of the RFI contamination in the astronomical data, as well as construction of the corrections to be applied to the astronomical spectra. The method could be generalized (1) to interferometer arrays, (2) to correct for scattered solar radiation that causes spectral "standing waves" in single-dish spectroscopy, and (3) to pulsar survey and timing applications where a digital correlator plays an important role in broadband pulse dedispersion.

This technique does not require "clean copies" of the RFI signal, since the method is immune to the effects of multipath scattering in both the astronomy and reference signal channels, provided the multipathing does not lead to near perfect cancellation of the reference signal through destructive interference. The RFI signal paths obey simple phase and amplitude closure relations. Tests made at Parkes, demonstrate that a specifically designed reference sensor provides a higher signal-to-noise ratio reference signal – and consequently cleaner cancellation – than that obtained from a second horn feed at the Parkes Telescope focus, whose principal function is to illuminate the Parkes dish.

Subject headings: instrumentation: detectors — Methods: analytical, interference suppression

1. Introduction

The growing level of radio frequency interference (RFI) is a recognized problem for research in radio astronomy. Fortunately, the technological advances that are giving rise to the increasing background of radiation – through increased telecommunications and wide-spread use of high speed electronics – are also providing some of the tools necessary for separating astronomical signals from undesirable RFI contamination. New radio telescopes will necessarily have RFI suppression, excision and cancellation algorithms intrinsic to their designs. No one technical solution will make radio observations immune to interference; successful mitigation is most likely to be a hierarchical or progressive approach throughout the telescope, combining new instrumentation and algorithms for signal conditioning and processing (Ekers & Bell 2000; Ellingson 1999).

Techniques from the communication industry that are finding application in radio astronomy experiments include (1) adaptive beam forming with array telescopes that steer nulls of the instrument reception pattern in the directions of sources of RFI (Hampson et al. 1998; Ellingson & Hampson 2000; Lesham et al. 2000; Smolders & Hampson 2000; Kewley et al. 2000), (2) parametric signal modeling techniques, where the RFI signal is received and decoded to obtain a high signal-to-noise ratio (SNR) reference signal for subtraction from the astronomical data (Ellingson et al. 2000; Lesham & van der Veen 1999a; Lesham & van der Veen 1999b), and (3) adaptive filtering using a reference horn to obtain a high SNR copy of the RFI for real-time cancellation from the signal path ahead of the standard radio astronomical backend processors (Barnbaum & Bradley 1998).

This paper describes an intuitive but powerful RFI cancellation technique that is suitable for radio spectroscopy where time-averages are recorded. The method requires computation of cross power spectra between the RFI contaminated astronomical signals and high signal-to-noise ratio RFI "reference signals" obtained from a receiving system that senses the RFI but not the astronomical signal. The correction term that removes the unwanted RFI results from closure relations obeyed by the RFI signal. The test applications reported here derived the reference signal either from a separate horn antenna aimed at the RFI source or from a second feed horn at the focus of the Parkes telescope, as illustrated in Fig 1. For these experiments, we recorded digitally sampled baseband signals from two polarizations for both the reference and astronomy feeds, and then we performed the cross correlations in software off-line. However, the method could use correlation spectrometers of the sort already in use at radio observatories, and with minor design enhancements, future generation correlators could incorporate this technique with the additional benefit of the faster electronics, greater digital precision, and higher data rates that technological advance promises.

There are a number of advantages to performing this type of "post-correlation" RFI subtraction:

1. Provided the required correlation products are recorded (i.e. the online system is capable of recording correlation functions with a sufficiently large number of delay lags), the RFI subtraction can be performed offline, where it remains an option in the data reduction path, rather than a com-

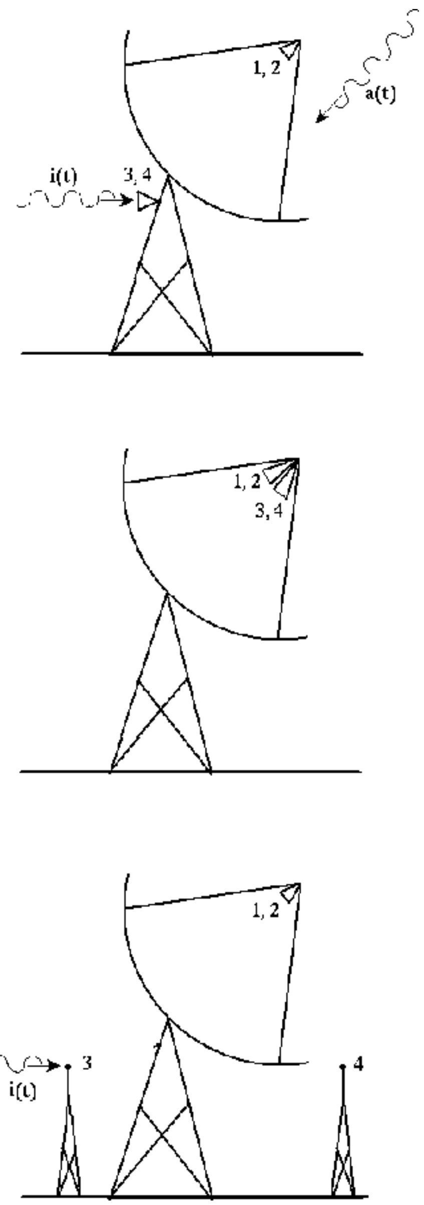

Fig. 1.— Three configurations applicable to the analysis in this paper. *Top* The four basebands are recorded from the 2 polarizations of the Parkes telescope feed and 2 polarizations of a reference horn directed at the RFI source. *Center* The four basebands correspond to 2 polarizations from each of two Parkes feeds. *Bottom* A proposed system for optimal application of the RFI subtraction technique described here.

mitment made online and permanently.

2. The method is not vulnerable to the effects of sporatic RFI, which hurt many algorithms that have an initialization period while they acquire the RFI signal and optimize their cancellation parameters.

3. Nor is the result influenced by changes in beam shape during adaptive nulling.

4. The correlation method is effectively a coherent subtraction, since the correlation functions retain the information describing relative phase between the RFI entering in the astronomy data stream and the RFI entering the reference antenna. As we show later, this means that the RFI noise power is largely subtracted, leaving only the usual components of system noise.

5. A modification of the method can be applied to pulsar data streams in which a digital correlator replaces the narrow band filter bank used in compensating for pulse dispersion.

6. The method can be generalized to removal of solar radiation whose multi-path scattering effects give rise to the spectral "standing wave" problem.

7. The present generation of digital correlators, which typically operate with single bit to 9 level precision, could implement this method for use in moderate levels of RFI for testing and astronomical observation in the near future.

The disadvantages of the method are: (1) The data rates will be high, since the method requires a full-scale cross correlator, preferably with multibit precision to accept large SNR RFI reference signals, that must dump spectra after relatively short integrations of less than $\sim$1 sec. Of course, these data rates are lower than recording the full baseband, but they are substantially higher than a real-time adaptive filter approach, which would allow long spectral integrations once the RFI has been canceled. (2) When the interference is much stronger than the astronomical signal, a 1 or 2 bit sampler is "captured" so that the data stream consists primarily of ± 2, and the zero crossings are determined by the phase of the interferer. Under these conditions, the astronomical data will be largely lost. These applications will require correlators with greater digital precision.

This paper provides a description of the post-correlation RFI cancellation technique and illustrates its success with data from the Parkes telescope. A mathematical overview shows (1) why unknown multipaths do not cause the algorithm to break down, (2) how to simply construct a suitable RFI reference spectrum, and (3) how to build an inverse filter to obtain immunity to low signal levels at frequencies that suffer destructive interference by multipathing in the reference horn signal path. A small simulation indicates that coarse digitization of the RFI reference signal may limit the achievable precision of RFI subtraction for this type of experiment.

2. The test data

The astronomical data used in testing these algorithms is a dual linear polarization data stream from the CSIRO ATNF 64m telescope at Parkes in Australia. One configuration has two polarizations from the central beam of the the Parkes multibeam receiver (Staveley-Smith et al. 1996) and two polarizations from a reference horn aimed at an interfering source (Bell et al. 2000). A second configuration uses both polarizations from two beams of the Parkes Multibeam system, which are directed at slightly different areas of the sky. The center frequency of the datasets was 1499 MHz in each case.

The datasets we used are labeled SRT00501, SRT00502 and SRT00601 (Bell et al. 2000). The main interfering source is a NSW Government digital point-to-point microwave link. Examples of the time-averaged spectrum for the RFI signal are shown in Fig 2. Further details are available in the ACA databases (Australian_Communications_Authority 1998; Sarkissian 1999). The 4 signals were downconverted to base band and passed through 5 MHz low pass filters. Each signal was then digitized with 2-bit precision at a 20MHz sampling rate to achieve a factor 2 oversampling and recorded using the CPSR recorder (van Straten et al. 2000). This dataset and others are freely available for conducting signal processing experiments (Bell et al. 2000). A description of some utility software for analyzing this dataset and some illustrations to assess the nature of the data are available from the authors.

3. Mathematical justification of the method

Here, we make the assumption that the RFI source emits a single signal $i(t)$. (At the RFI

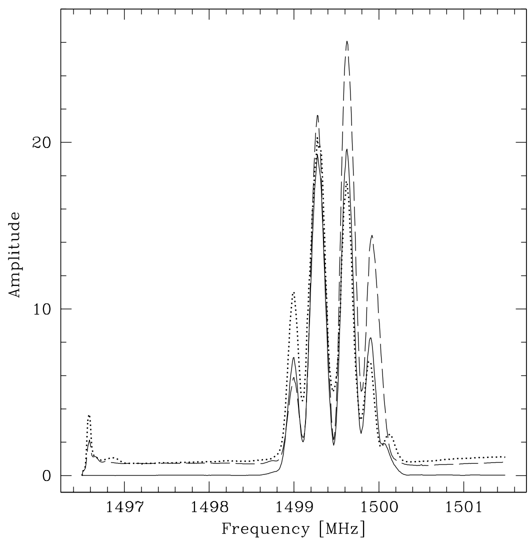

Fig. 2.— Scan averaged RFI spectra measured with the reference horn for scan SRT00502. Solid line is the cross power spectrum $C_{34}(f)$ defined in Eqn 8. Dashed and dotted lines indicate the auto-correlation spectra $P_3(f)$ and $P_4(f)$ in Eqn 6. The spectra have been passband calibrated using approximate gain curves for the 5 MHz filters. There are 512 frequency channels covering a 5 MHz band.

source, the signal from a single power amplifier feeds an antenna of unknown, but irrelevant, polarization.) The RFI that appears differently in the recorded data channels at Parkes has experienced scatterings with different path lengths and amplitudes, so that the received signals are linear sums of time delayed versions of the original broadcast $i(t)$.

There are four signal paths s_1, s_2, s_3, and s_4 to consider: the two astronomical channels, $s_1(t)$ and $s_2(t)$, which convey the voltages $a_A(t)$ and $a_B(t)$ from the celestial sources for the two independent polarizations from the Parkes Telescope receiver along with contamination from the RFI signal $i(t)$, and two channels $s_3(t)$, and $s_4(t)$ containing the representations of $i(t)$ but negligible signal from the celestial sources. All the signals are vulnerable to corruption by stochastic noise $n_1(t)$, $n_2(t)$, $n_3(t)$, $n_4(t)$ and distortions due to multipath propagation. For example, the measured signal in channel 1 comprises channel noise, plus the convolutions of the impulse responses for the multiple scattering paths for the interference signal and the true astronomy signal: $s_1(t) = H_A(t) * a_A(t) + H_1(t) * i(t) + n_1(t)$. Here $H_A(t)$ and $H_1(t)$ are impulse responses for the astronomy signal path and interference respectively.

For many purposes, an intuitive picture of the multipathing results from considering the scattering sites to be achromatic mirror-like scatterers each with relative effective areas $G_{A,j}$ and $G_{1,k}$, and attaching the path delay to each separate version of the astronomy and RFI signals, $s_1(t) = \sum_j G_{A,j} a_A(t - \tau_{1,j}) + \sum_k G_{1,k} i(t - \tau_{1,k}) + n_1(t)$. The time delays τ are determined by the different path lengths $L_{1,j}$ to give $\tau_{1,j} = L_{1,j}/c$, where c is the speed of light.

In this experiment, the goal is to explore the usefulness of cross-correlation spectra to correct for the effects of RFI in time-averaged spectra. The data processing for these tests simulates a radio astronomy backend by computing power spectra and cross power spectra in software. The sampled voltages are treated in 8192 sample blocks (410μsec durations). Fourier transformation of each block produces a spectrum of 4096 independent complex coefficients. These spectra are scaled sums of the of the Fourier transforms of the astronomy signals, the RFI and noise:

$$\begin{aligned} S_1(f) &= g_A A_A + g_1 I + N_1 \\ S_2(f) &= g_B A_B + g_2 I + N_2 \\ S_3(f) &= g_3 I + N_3 \\ S_4(f) &= g_4 I + N_4 \end{aligned} \tag{1}$$

contain contributions from the celestial sources ($A_A(f)$ and $A_B(f)$), the RFI ($I(f)$), and the noise in each channel ($N_i(f)$), modulated by the associated complex voltage gains, which are the Fourier transforms of the impulse responses $H(t)$. Here, the gains for each channel separate into dependencies on (1) the path delay L/c, which appears in a frequency dependent phase term, according to the Shift Theorem of Fourier transforms, and (2) a possible additional frequency dependence $g(f)$ of each delay path:

$$g_1(f) = \sum g_{1,k}(f) e^{i2\pi f L_{1,k}/c} \tag{2}$$

In fact, the complex gain and delay factors are sufficiently general to include complicated scatterers and propagation through dispersive and lossy media. As a special case, consider a situation with only two propagation paths with gains whose amplitudes and phases are independent of frequency (i.e., g_α and g_β constant and real):

$$\begin{aligned} g(f) &= g_\alpha e^{i2\pi f L_\alpha/c} + g_\beta e^{i2\pi f L_\beta/c} \\ &= 2g_\alpha e^{i\pi f(L_\alpha+L_\beta)/c} \cos\left(\frac{\pi f(L_\alpha - L_\beta)}{c}\right) \\ &\quad +(g_\beta - g_\alpha) e^{i2\pi f L_/c} \end{aligned} \tag{3}$$

The power gain is

$$\begin{aligned} |g(f)|^2 &= g_\alpha^2 + g_\beta^2 \\ &\quad +2g_\alpha g_\beta \cos\left(\frac{2\pi f(L_\alpha - L_\beta)}{c}\right) \end{aligned} \tag{4}$$

which oscillates between $(g_\alpha + g_\beta)^2$ and $(g_\alpha - g_\beta)^2$ as a function of frequency. If the gains are equal for the two paths, $g_\alpha = g_\beta = g_o$,

$$|g(f)|^2 = 4g_o \cos^2\left(\frac{\pi f(L_\alpha - L_\beta)}{c}\right) \tag{5}$$

the gain is modulated by a cosine function of the difference in path length. For the data being analyzed here, it is not clear whether the modulation of the RFI spectrum seen in Fig. 2 indicates this interference effect or whether it is a consequence of an intrinsic modulation scheme for carrying information on this signal.

The real power spectra for the four data channels have the following form, once terms that average toward zero are omitted and the complex gains are assumed to be constant over the time span for which the spectra are computed:

$$\begin{aligned} P_1(f) &= < S_1 S_1^* > \\ &= |g_A|^2 < |A_A|^2 > \\ &\quad + |g_1|^2 < |I|^2 > + < |N_1|^2 > \\ P_2(f) &= < S_2 S_2^* > \\ &= |g_B|^2 < |A_B|^2 > \\ &\quad + |g_2|^2 < |I|^2 > + < |N_2|^2 > \\ P_3(f) &= < S_3 S_3^* > \\ &= |g_3|^2 < |I|^2 > + < |N_3|^2 > \\ P_4(f) &= < S_4 S_4^* > \\ &= |g_4|^2 < |I|^2 > + < |N_4|^2 > \end{aligned} \tag{6}$$

We adopt a normalization where the power levels $< |A_A|^2 > \approx < |I|^2 > \approx < |N_1|^2 >$ so that, for example, in data channel 1 the signal to noise ratio $SNR_1 \sim |g_A|^2$, and the interference to noise ratio $INR_1 \sim |g_1|^2$.

Examples of the power spectra are shown in Fig 3, which has averages of the power spectra for a full 25 sec integration. Since the data are $2\times$ oversampled, we kept the total power and cross power spectra of the lower 2048 complex Fourier coefficients, and then block averaged by 4 to keep power spectra of length 512 spectral channels for further manipulation at 9.8 kHz resolution.

This discussion has assumed that the complex gain terms are constant over the integration time, allowing us to separate the interference from the gain in expressions such as:

$$< g_1 I g_1^* I^* > = |g_1|^2 < |I|^2 > \tag{7}$$

In anticipation of the discussion of section 5 we note that this assumption will fail for extended integration times since the scattering paths that lead the RFI signal to the telescope feed will change, resulting in loss of precision in the cancellation scheme and and leading to substantial residuals in the corrected spectra.

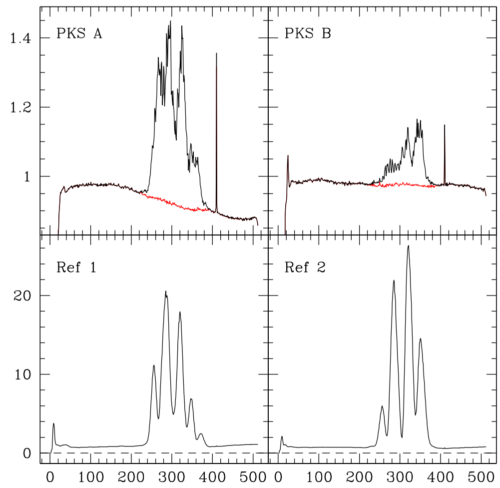

Fig. 3.— The Power Spectra PKS A= $P_1(f)$, PKS B= $P_2(f)$, Ref 1= $P_3(f)$, and Ref 2= $P_4(f)$ for scan SRT00502. These spectra are the averages of ∼25 seconds of data. A passband calibration has been applied to compensate for the gain dependence of the 5 MHz band limiting filters. The upper panels show the spectra both before and after cancellation.

The complex cross power spectra for all combinations of the four data channels have the following form when the leading contributions are retained:

$$\begin{aligned}
C_{12}(f) &= \; < S_1 S_2^* > \\
&= g_A g_B^* < A_A A_B^* > \\
&\qquad + g_1 g_2^* < |I|^2 > \\
&\qquad + g_1 < I N_2^* > + g_2^* < N_1 I^* > \\
&\qquad + < N_1 N_2^* > \\
C_{ij}(f) &= \; < S_i S_j^* > \\
&= \qquad + g_i g_j^* < |I|^2 > \\
&\qquad + g_i < I N_j^* > + g_j^* < N_i I^* > \\
&\qquad + < N_i N_j^* > \\
&\qquad \text{for i} \neq \text{j}, \;\; \text{j} > 2 \qquad (8)
\end{aligned}$$

Examples of these cross power spectra are shown in Fig 4. The narrow tone standing out strongly in channel 410 in C_{12} is also weakly present in the other cross power spectra. Both C_{12} and C_{34} have broadband correlated power, which is clear in the integrated spectra both as a significant non-zero amplitude and as a well defined trend in phase across the band. The phase gradients that are clearly visible in the $C_{13}(f), C_{14}(f), C_{23}(f)$, and $C_{24}(f)$ spectra indicate differential path delays. The delay for $C_{13}(f), C_{14}(f)$ and for the channel numbers above 300 in $C_{23}(f)$, and $C_{24}(f)$ amounts to 15 time steps (0.75μsec). The steeper phase gradient for channels below 300 in $C_{23}(f)$, and $C_{24}(f)$ imply path delays of 60 time steps = 3μsec or a path length of ∼900m. Apparently, the frequency dependent reception pattern of the far sidelobes of the Parkes dish, coupled with complicated scatterers in the field, can lead to quite complex spectral dependence for the RFI. A strength of our method is the simplicity with which it handles this complex multipathing. It was the rapid phase winding seen in the 512 channel display (9.8 kHz resolution) in Fig 4, that lead to expanding from 2048 to 8192 sample FFTs (to obtain 2.4 kHz resolution) with a significant improvement in the effectiveness of the algorithm.

Fig. 2 compares three time-averaged power spectra representing the RFI signal sensed by the reference horn: power spectra for each of the two polarizations and one cross power spectrum. For

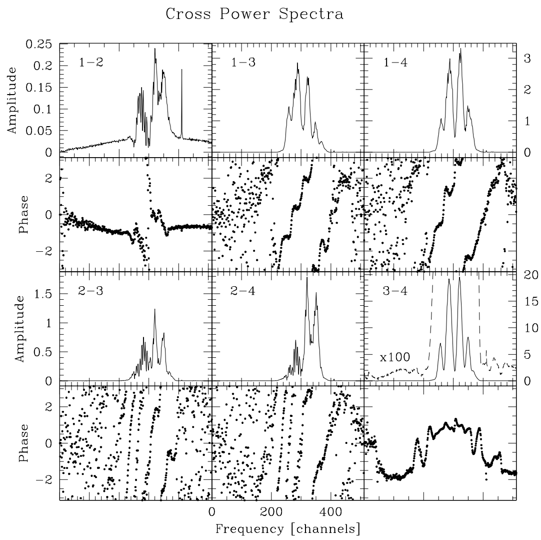

Fig. 4.— The Cross Power Spectra $C_{12}(f), C_{13}(f), C_{14}(f), C_{23}(f), C_{24}(f)$, and $C_{34}(f)$ for scan SRT00502. These spectra are the averages of ∼25 seconds of data. The spectrum $C_{34}(f)$ at lower right is also plotted with a rescaling of a factor of 100 in order to display the noise level away from the frequencies containing strong RFI.

use in correction schemes, the cross power spectrum should have the advantage that it is not contaminated by the positive bias of the receiver noise total power that is seen in the autocorrelation power spectra. In practice, the low level correlated signal, due to actual cross correlated broadband power or due to correlated quantization noise, may be a limit to the accuracy of the cross power spectrum as an estimate of the RFI.

The correlation spectra formed in Eqn 8 combine to form estimates of the RFI contamination in the three spectra measured by the Parkes Telescope:

$$|g_1|^2 < |I|^2 > \; = \; \frac{g_1 g_3^* g_1^* g_4}{g_3^* g_4} < |I|^2 > \; \approx \; \frac{C_{13} C_{14}^*}{C_{34}^*} \tag{9}$$

$$|g_2|^2 < |I|^2 > \; = \; \frac{g_2 g_3^* g_2^* g_4}{g_3^* g_4} < |I|^2 > \; \approx \; \frac{C_{23} C_{24}^*}{C_{34}^*} \tag{10}$$

$$g_1 g_2^* < |I|^2 > \; = \; \frac{g_1 g_4^* g_2^* g_3}{g_3 g_4^*} < |I|^2 > \; \approx \; \frac{C_{14} C_{23}^*}{C_{34}} \tag{11}$$

The appearance of the C_{34} term in the denominator for Eqns 9-11 may indicate there will be a problem in implementing a correction scheme in frequency ranges where C_{34} (as plotted in Fig 2) becomes small or zero. In many situations when the signal to noise ratio for the spectra in the numerator is very high, the cross power spectra in the numerator will also be small or zero whenever C_{34} is small, so that divergence would be canceled. A common method used in Weiner filters to avoid division by small numbers in the presence of noise in this kind of situation is to create a filter of the following form:

$$|g_1|^2 < |I|^2 > \; \approx \; \frac{C_{13} C_{14}^* C_{34}}{\psi(f) + C_{34} C_{34}^*} \tag{12}$$

$$|g_2|^2 < |I|^2 > \; \approx \; \frac{C_{23} C_{24}^* C_{34}}{\psi(f) + C_{34} C_{34}^*} \tag{13}$$

$$g_1 g_2^* < |I|^2 > \; \approx \; \frac{C_{14} C_{23}^* C_{34}^*}{\psi(f) + C_{34} C_{34}^*} \tag{14}$$

where $\psi(f)$ is the square of the power spectrum of the noise present in $C_{34}(f)$. In practice, during these experiments described here, a constant

ψ_0 was used in place of $\psi(f)$. Whenever $\psi(f)$ becomes small compared to $C_{34}(f)$, the expressions Eqns 12-14 revert to Eqns 9-11. When the noise exceeds the signal power in C_{34}, the computed correction tends to zero.

Examples of these complex correction spectra are shown in Fig 5. The spectra for Correction A and Correction B have zero phase over the spectral range where the signal is significantly non-zero. Since these corrections are expected to be real valued according to Eqns 9-11, the occurrence of zero phases is a statement of phase closure for these correlation spectra. Note that the denominators of Eqns 12-14 are purely real, and the numerators, such as $C_{13}C^*_{14}C_{34}$, form logical triangles for computing closure phases.

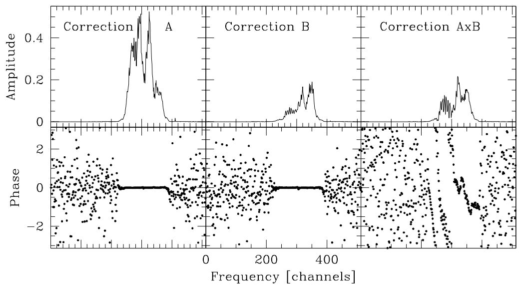

Fig. 5.— The Complex Correction Spectra derived from Eqns 12-14 for scan SRT00502 for application to the Parkes spectra A, B, and A×B. These plots show the averages of ∼25 seconds of data. The RFI subtraction was actually performed on 82 msec averages. A & B indicate the 2 polarizations.

A closure relation

$$\frac{C_{13}C_{24}}{C_{23}C_{14}} = \frac{g_1 g_3^* g_2 g_4^*}{g_2 g_3^* g_1 g_4^*} = 1 \tag{15}$$

can also be constructed and tested. It too will suffer from divergence of the quotient in frequency ranges where the cross power spectra are noisy and C_{23} and C_{14} have small amplitude. Here we avoid including C_{12}, which has significant cross correlated power in addition to the RFI signal. Fig 6 shows averages of the closure quantity, plotted as amplitude and phase across the spectrum. There is deterioration in the closure relation when the RFI signal is low, as expected.

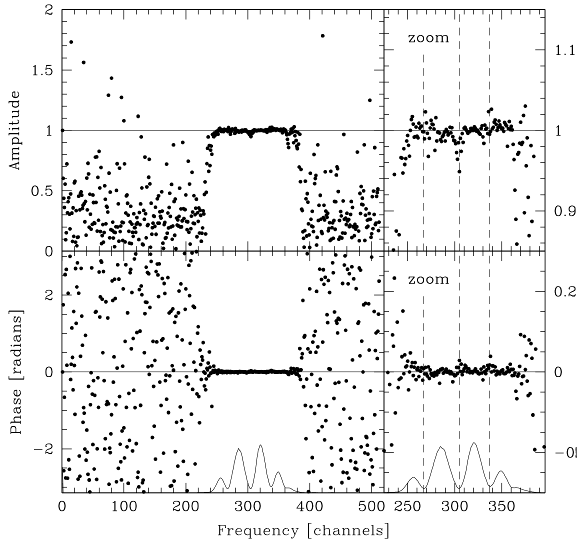

Fig. 6.— The complex closure quantity $C_{13}C_{24}/C_{23}C_{14}$ averaged for scan SRT00502. *Left*: full spectrum. *Right*: expanded scales. Reduced scale plots of the average RFI cross power spectrum from Fig 2 are drawn in the bottom panels for comparison.

Figure 7 shows a block diagram summary how the astronomical and reference signals are combined and processed to perform the RFI cancellation.

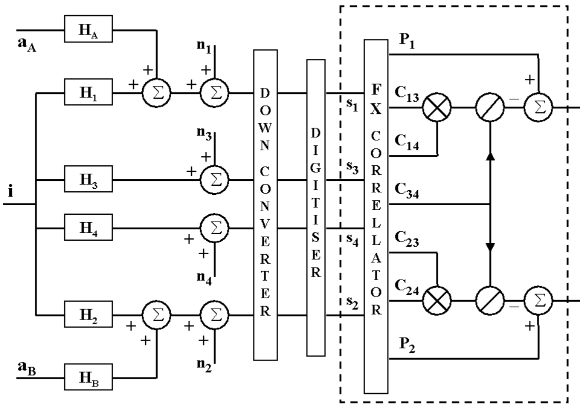

Fig. 7.— Block diagram showing the signal conditioning and processing applied to the signals. The block enclosed by the dashed line is implemented entirely in post processing software. Signals flow left to right on all horizontal lines. The symbols are described in the text of the paper. The operations applied to C_{34} after the correlator are summarized in Eqns 12 and 13.

4. Noise and the Accuracy of the Cancellation

In this section we assess the importance of the Interference-to-Noise ratio. First we expand the autocorrelation spectra, keeping all cross terms, including those that average toward zero. Then $P_1(f)$ becomes

$$\begin{aligned} P_1(f) &= |g_A|^2 < |A_A|^2 > + |g_1|^2 < |I|^2 > + 2\mathrm{Re}\,[g_1 g_A^* < IA^* > + g_1 < IN_1^* >] \\ &\quad + 2\mathrm{Re}\,[g_A < AN_1^* >] \, + < |N_1|^2 > \end{aligned} \tag{16}$$

The complex correction spectra were described by equations 9, 10 and 11. Including the cross terms and noting that when

$$g_3 \text{ and } \mathrm{g}_4 >> \mathrm{g}_1 \text{ and } \mathrm{g}_2 \tag{17}$$

and the interference power to noise power ratios

$$\begin{aligned} INR_3 &= \frac{|g_3|^2 < |I|^2 >}{< |N_3|^2 >} \approx |g_3|^2 \quad >> \; 1 \\ INR_4 &= \frac{|g_4|^2 < |I|^2 >}{< |N_4|^2 >} \approx |g_4|^2 \quad >> \; 1 \end{aligned} \tag{18}$$

then the correction CX_1 for $P_1(f)$ becomes:

$$\begin{aligned} CX_1 &\approx \frac{C_{13} C_{14}^*}{C_{34}^*} \\ &\approx |g_1|^2 < |I|^2 > + 2\mathrm{Re}\,[g_1 g_A^* < IA^* > + g_1 < IN_1^* >] \\ &\quad + \frac{g_A g_1^*}{g_3^*} < AN_3^* > + \frac{g_A^* g_1}{g_4^*} < A^* N_4 > \\ &\quad + \frac{g_1^*}{g_3^*} < N_1 N_3^* > + \frac{g_1}{g_4} < N_1^* N_4 > - \frac{|g_1|^2}{g_3^* g_4} < N_3^* N_4 > \end{aligned} \tag{19}$$

The terms in Eqn 19 involving I all appear in the power spectrum of Eqn 16, so that application of this correction CX_1 to $P_1(f)$ leads to a result with no residual contamination by the RFI:

$$\begin{aligned} P_1(f) \; - \; CX_1 &= |g_A|^2 < |A_A|^2 > + \; < |N_1|^2 > \\ &\quad + 2\mathrm{Re}\,[g_A < AN_1^* >] \; - \; \frac{g_A g_1^*}{g_3^*} < AN_3^* > - \frac{g_A^* g_1}{g_4^*} < A^* N_4 > \\ &\quad - \frac{g_1^*}{g_3^*} < N_1 N_3^* > - \frac{g_1}{g_4} < N_1^* N_4 > + \frac{|g_1|^2}{g_3^* g_4} < N_3^* N_4 > \end{aligned} \tag{20}$$

The complete cancellation of the RFI terms is consistent with the concept that post correlation subtraction is equivalent to coherent subtraction of the RFI electric field $i(t)$ in the time domain, which should leave no trace of the RFI signal nor an increase in noise power. Provided the INR for the reference horn channels is substantially greater than the INR for the Parkes feed channels, the noise terms due to N_3 and N_4 will be smaller by a factor of order $\beta \sim \sqrt{INR_3/INR_1} \approx |g_3|/|g_1|$ than the normal noise contributions arising from N_1 plus the astronomical signal power. The terms other than $|g_A|^2 < |A_A|^2 >$ and $< |N_1|^2 >$ shown in Eqn 20, such as $(g_A^* g_1/g_4^*) < A^* N_4 > \propto |g_A| \beta^{-1} t^{-1/2}$ and $(g_1^*/g_3^*) < N_1 N_3^* > \propto \beta^{-1} t^{-1/2}$ average toward zero (in inverse proportion to the square root of the integration time), provided the noise in the signal channels is independent. The next higher order terms, which are not included in Eqn 20, have dependencies such as $< IN_1^* >< N_1^* N_4 > /g_4 < |I|^2 > \propto t^{-1}$ and $g_1^* < IN_3^* >< I * N_1 > /g_3^* < |I|^2 > \propto \beta^{-1} t^{-1}$, which converge toward zero faster than the dominant noise terms.

5. Application of RFI Subtraction

RFI subtraction for the total power spectra proceeds by computing the correction spectra indicated in Eqns 12- 13 and then subtracting the real parts of the correction power from the autocorrelation spectra. For the purposes of display in Fig 8, the resulting spectra are normalized by dividing the spectra by gain templates formed from the scan average of the total power spectra of scan SRT00601, which was recorded while the sky frequency for the Parkes data channels was tuned off the RFI frequency. Since this gain template is in common to the processing for both scans SRT00501 and SRT00502, some of the fine scale noise bumps and simularity of the spectra summarized in Fig 8 may result from this common gain template.

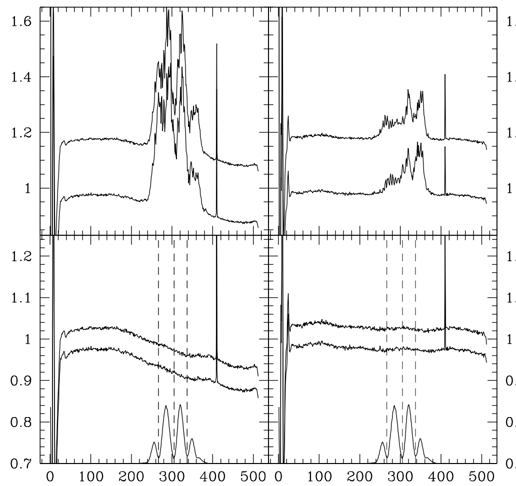

Fig. 8.— Comparison of two scans: SRT00501 and SRT00502. *Upper Panels:* Uncorrected power spectra for the two Parkes polarizations. Spectra for SRT00501 are displaced vertically by 0.2 in amplitude. *Lower Panels:* Corrected power spectra for the two Parkes polarizations. Spectra for SRT00501 are displaced vertically by 0.05 in amplitude. Reduced scale copies of the RFI cross power spectrum are included for reference with vertical dashed lines to indicate the minima in the RFI spectrum.

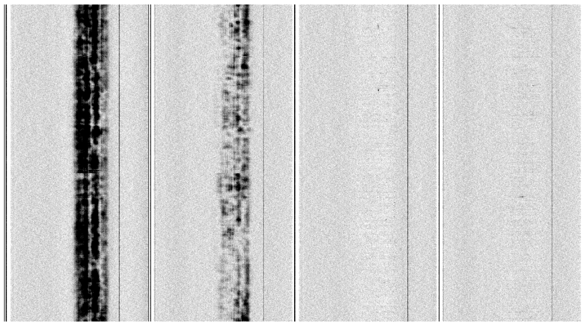

Fig. 9.— Dynamic Power Spectra over 564 time steps of 82 msec each (Scans SRT00501 and SRT00502). There are four spectra plotted in parallel with time increasing vertically. *Left* The two Parkes polarizations prior to RFI subtraction. *Right* The two Parkes polarizations after RFI subtraction. All spectra are passband calibrated to compensate for the frequency dependence of the 5 MHz filters. A third order polynomial spectral baseline was fitted to channels 30-235, 370-405 and 420-500 and subtracted for each time step.

The time dependence of the RFI sensed by the Parkes telescope is plotted in image format in Fig 9, side by side with the spectra resulting from the RFI subtraction. These spectra received the same processing as described for the averages in Fig 8, with the additional step of subtracting a third order polynomial spectral baseline from each time step. This additional step was done to remove some faint variations in the total power level that occurred from one integration to the next. The variation prevented effective use of the RMS variation in each channel as a function of time to indicate how well the RFI subtraction algorithm had worked.

There are only small residuals left in the corrected spectra, scarcely visible in the noise. Measurement of the RMS deviation as a function of time for each channel (see Fig 11 below) shows that there are a few channels with RMS fluctuation as much as a factor $\sim$1.8 above the typical noise level across the spectrum.

The polarized flux sensed by the Parkes polarizations A and B is shown in the cross power spectra in Fig 10. The figure includes the raw spectrum and the corrected spectrum after subtraction of the correction shown in Fig 5. Remaining in the corrected spectrum, there is a slow modulation of the power across the 5 MHz band, probably indicating that this power represents broad band noise signal that is scattered within the Parkes telescope structure with the same delay path lengths associated with traditional standing waves and path lengths of a few hundred feet.

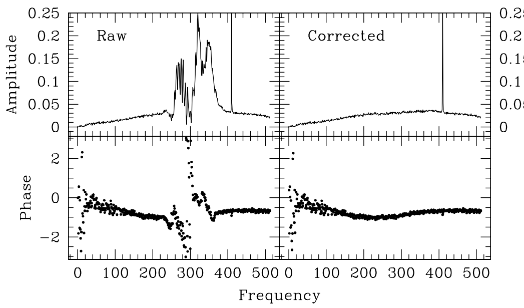

Fig. 10.— Raw and Corrected Parkes A×B cross power spectra. *Left*: The raw, complex cross power spectrum. *Right*: The corrected complex spectrum.

Figure 11 shows how varying the ψ_o factor defined for use in Eqns 12-14 affects the autocorrelation spectra. In all cases, the correction procedure operated on 82 msec averages, followed by calibration, subtraction of a spectral baseline, and formation of the grand averages that are displayed. The RMS deviation was computed for each channel as a function of time in order to sense the variability of the residual RFI signal left after application of the algorithm. The figure shows that the choice of $\psi_o = 0$ has the expected effect of drastically raising the noise level where the RFI is weak. Once ψ_o is increased above 0.001 little change in the character of the result can be seen, although there is a slight reduction in noise level outside the RFI contaminated frequency ranged as the ψ_o goes to 0.1. The spectrum inside the contaminated range is unchanged over the entire range of ψ_o.

The integration time over which the RFI cor-

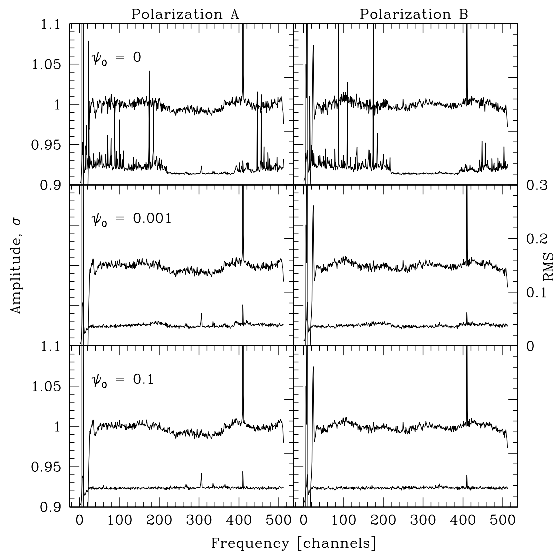

Fig. 11.— The effect of varying the ψ_o factor defined for use in Eqns 12-13. For all cases, the algorithm was applied to 82 msec integrations. In each panel, the upper spectrum shows the corrected, calibrated, baselined spectrum; the lower spectrum is the RMS scatter about the mean spectrum for each channel. *Top*: $\psi_o = 0$. *Center*: $\psi_o = 0.001$. *Bottom*: $\psi_o = 0.1$.

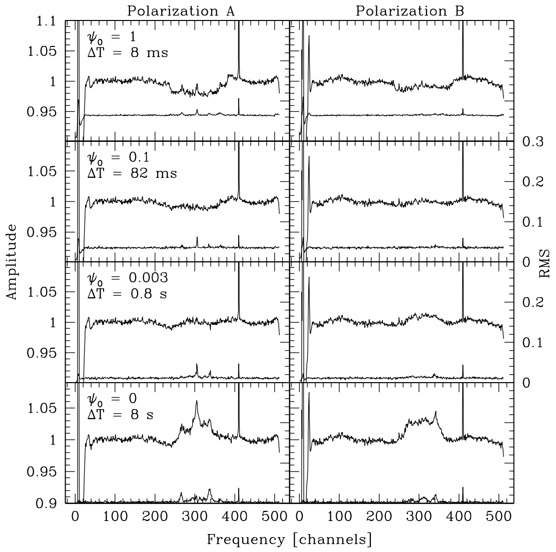

Fig. 12.— The effect of varying the time interval on which algorithm described in Eqns 12-14 is applied. The interval varies from 8 msec to 8 sec in factors of 10. In each panel, the upper spectrum shows the corrected, calibrated, baselined spectrum; the lower spectrum is the RMS scatter about the mean spectrum for each channel as a function of time. The typical value for RMS should decrease by $\sqrt{10}$ for each increase in factor 10 in integration time.

rections are applied is a critical parameter when the signal to noise ratio of the reference signal data path is low. If the integration time is too short, then some of the derived correction will be noise, and this will be folded into the resulting spectrum. On the other hand, if the integration time is long, the impulse response functions that couple the astronomy and RFI signals to the receiver will vary, and the mathematics in Eqn 7 and Eqns 9-11 will break down. Fig 12 shows a series of tests with a range of integration times (8 msec to 8 sec) for application of the RFI subtraction. In all cases, the plots give the grand averages of the entire 25 seconds of the scan after application of the algorithm on the shorter data segments. The parameter ψ_o has an appropriate value in each case to produce a stable noise level and representation of spectral features in the frequency range away from the RFI contamination. For these data, the algorithm was most effective for integration times of only a ~ 1 sec or less. When treated on 8 sec averages, substantial RFI remains unsubtracted.

6. Discussion of Limitations

Several factors can enter to limit the precision of the cancellation:

1. Clearly, a noisy or non-linearly distorted reference signal will lead to imprecise cancellation as shown in Eqn 20. Spurious RFI resulting from non-linear mixing of very strong signals in the receiver cannot be removed by this direct method.

2. A wide range of delays for the scattered RFI led to problems in our initial experiments, which simulated an FX correlator with 2048 sample transforms. The RFI illustrated in Fig 4 has two strong components that are delayed by 15 and 60 time steps. A 60 time step delay is ~3% of the time block being processed, so that the cross correlation is not being performed on fully overlapped data streams. Increasing the window to 8192 was adequate to reduce the residuals to a level that was barely visible above the noise in the corrected spectra. An additional but less significant improvement resulted from applying an constant delay offset of 35 time steps to the reference signal at the input to the "FX correlator" to make it closer to the average of the principal delays in the Parkes data channels. A traditional time-domain lag correlation spectrometer would not encounter

this problem, provided a sufficient number of lags are allocated to fully cover the range of delays experienced by the RFI.

3. In these tests at Parkes, there is a possibility that some uncancelled signal may be present due to a second transmitter operating at these same frequencies. The reference horn was pointed at the stronger, nearby transmitter, while the second transmitter, located at approximately three times the distance, can be scattered into the Parkes Telescope signal paths without being sensed by the reference horn.

4. The coarse digitization of the RFI reference signals will eventually form a limitation to the precision of the subtraction. Crude quantization generates an artificial noise floor throughout the spectrum, effectively scattering power out of the narrow band RFI. Since both polarizations from the reference horn are recorded at relatively high signal to noise ratio, the quantization noise is also correlated between the two data channels, so that there is corruption of the cross power spectrum as well as for the autocorrelation spectra. (This is essentially saying that the term $< N_3 N_4 >$ in Eqn 8 does not average to zero with increased integration.)

Simple simulations in Fig 13 demonstrate the effect of coarse digitization. The simulation generates total power (autocorrelation) spectra formed analogously to those measured in this experiment from time series that are oversampled by a factor of two. Gaussian noise, passed through a filter constructed with four parallel narrow Gaussian shaped filters, produces a power spectrum resembling the RFI power spectrum, as shown in the top panel of Fig 13. Two bit and single bit quantization of the filtered time sequence, followed by computation of the modulus-squared of the Fourier Transform, leads to the simulated autocorrelation spectra in the top panel of Fig 13, here shown normalized to unity at the peak. The 2 bit and 1 bit cases show noise floors at the ~0.3% (-22db) and ~0.6%(-25.6db) levels respectively. The figure also demonstrates that the valleys between the strong features become filled in after crude quantization. In this example, the 2 bit digitization loses more than 1 db (an increase of about 25% in the signal power level) in the valley. In a cross power spectrum, such as $C_{34}(f)$ in Eqn 9, an erroneously high level in the valley leads to a quotient that is

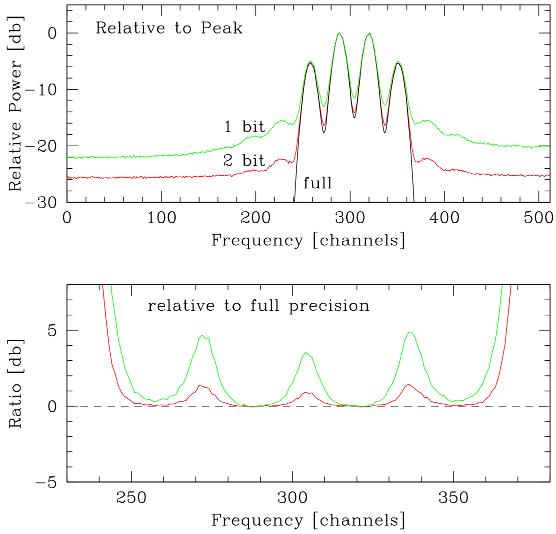

Fig. 13.— The effect of crude quantization of the RFI signal on total power spectra when the signal to receiver noise ratio is high. The effect is simulated by subjecting a data stream to different levels of quantization and then computing the power spectrum as described in the text. *Upper panel*: Comparison of spectra for 1 bit, 2 bit and full precision, normalized to unity at peak. *Lower panel*: Ratio of spectra computed using 1 bit and 2 bit digitization compared to full precision, for the limited channel range where the RFI signal is strong.

20% low, thereby underestimating the magnitude of the correction signal to be subtracted. This occurs systematically in the valleys, possibly contributing to the residuals seen in Fig. 8.

For the case of cross power spectra, the signals arrive with different gains and delays, causing the digitization to be a little different for the two signal paths (S_3 and S_4). This is the likely explanation of the observed noise floor of $\sim$0.2% observed for the cross power spectrum $C_{34}(f)$ plotted in Fig 4, which is significantly below the values simulated for the autocorrelation spectra.

7. The Toxicity Test

A crucial requirement of an RFI subtraction algorithm is that it must leave the astronomical signal of interest unaltered. To test the current method, we added simulated galaxy signals to the two Parkes input data streams. Independent gaussian noise was filtered with a double-horned galaxy profile and the instrumental IF filter passbands and injected into the data pipeline just before the correlation stage. Fig 14 shows a comparison between the RFI corrected spectra both with and without the galaxy. To highlight the difference between the injected signal and the output after RFI subtraction, the bottom panel shows (1) the difference between the output with and without the added signal and (2) the ratio of this difference to the synthetic galaxy profile added to the input. The RMS deviation of the ratio about unity is 0.005 for polarization A and 0.006 for polarization B. No systematic deviations are seen across the band, other than rises in noise level at the edges where the galaxy profile is approaching zero at the edge of the profile. The conclusion is that this method does no systematic harm to the astronomical signals.

8. The Parkes Two Feed Experiment

The mathematical description (Eqns. 6 to 14) can be equally well applied to using a second feed from the Parkes Telescope as the "reference horn," except that the data channels 3 and 4 may also be carrying astronomical signals. Since the feeds point different directions in the sky, these are independent astronomy signals, which will not correlate and therefore will not be subtracted from each other by this algorithm. The two feeds prob-

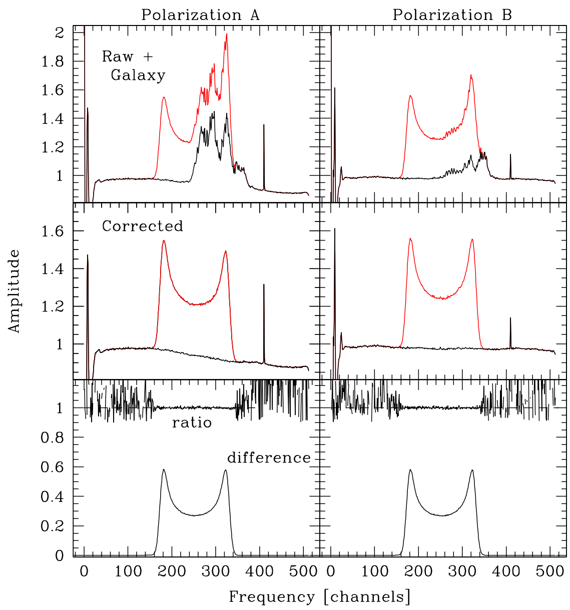

Fig. 14.— Survival of an injected synthetic galaxy signal in the astronomy channels through the RFI subtraction process. *Top*: Raw spectra – with and without the synthetic galaxy signal. *Center*: Corrected spectra – with and without the synthetic galaxy.. *Bottom*: Difference between the corrected spectra and the ratio between the input synthetic spectrum and the difference spectrum.

ably do sense the same RFI signal $i(t)$, although through different scattering paths. This is sufficient commonality that the cross power spectral approach should permit each feed to serve as the reference antenna for the other. Similar experiments have been reported (Sault 1997; Kewley et al. 1999).

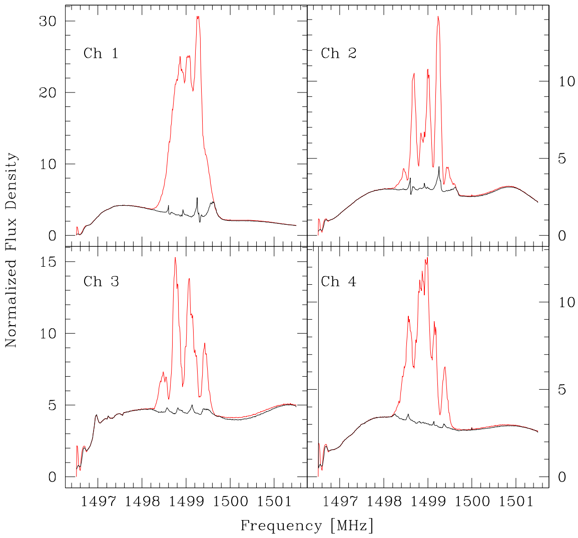

Fig. 15.— The autocorrelation spectra for both polarizations of two feeds of the Parkes Multibeam System before and after rfi subtraction. An attempt was made to apply a passband calibration using the same passbands determined from the scan SRT006_01 for the reference horn experiment. The data were treated in ~82 msec averages, which in turn were integrated over the 20 second duration of the scan.

Fig. 15 shows a comparison between the autocorrelation spectra measured for the Parkes two feed experiment, before and after RFI subtraction. There is noticeable difference among the four channels in the effectiveness of the RFI subtraction. This is likely to be a result of the greater broadband polarized flux or correlated noise in the cross polarized spectra 3×4 that is being used as the "reference" for data channels 1 and 2. As shown in Fig. 16, this noise floor is stronger in feed 2 ($INR \sim$ 35:1) than in feed 1 ($INR \sim$ 100:1), causing the rfi template spectra derived from the cross power spectra to be less faithful, which in turn leads to larger error in the correction spectra to be subtracted from feed 1. For comparison, the reference horn spectrum $C_{34}(f)$ in Fig 4 has $INR \sim$ 1000:1

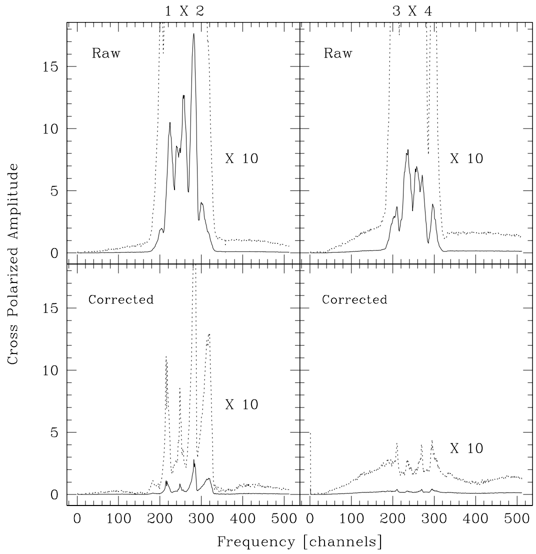

Fig. 16.— The cross polarization spectra for two feeds of the Parkes Multibeam System before and after rfi subtraction for scan SRT00108. An attempt was made to apply a passband calibration using the same passbands determined from the scan SRT006_01 for the reference horn experiment. The data were treated in ~82 msec averages, which in turn were integrated over the 20 second duration of the scan. Dotted lines show the spectra amplified by a factor 10.

9. Application to Pulsar Timing and Surveys

The most basic output of our cancelling system is the dynamic spectra, like those shown in Fig. 9. For spectral applications, we then average over time. For pulsar applications the length of the time bins in the dynamic spectra is a small fraction of the pulse period (e.g. 1 part in 100 or 1000). At this point the data looks just like what is obtained from an analog filter bank for example. The data can be processed using standard techniques (i.e. fold the data modulo the pulse period, then dedisperse, then average over frequency). Since we have demonstrated that technique works well for time bin scale as small as 8ms, this technique can be applied directly for slow pulsars (i.e. $P > 200$ms).

In the case of faster pulsars, (e.g. those with millisecond periods), the length of the time bins would be too short to obtain enough INR for the cancelling to work well. We see two possibilities to overcome this problem:

1. By doing some folding of the data at the pulse period before the cancellation and then completing folding afterwards.

2. By constructing a cross-power "coupling spectrum" $X(f)$ that is valid for the time during which the "g factors" of Eqn 1 are stable. For example:

$$X_{13}(f) = \frac{g_1^* g_4}{g_3^* g_4} \approx \frac{C_{14}^*}{C_{34}^*}$$

where C_{14} and C_{34} are averaged for up to 1 second as appropriate. Then the correction CX_1 can be computed and applied on shorter timescales:

$$CX_1 = |g_1|^2 < |I|^2 >= X_{13} g_1 g_3^* < |I|^2 >\approx X_{13} < S_1 S_3^* >$$

where $< S_1 S_3^* >= C_{13}$ and the corrections CX_1 are now evaluated and applied on short timescales compared to the pulsar period. The algorithm would use which ever of C_{13} and C_{14} have the higher INR or use the average resulting from both X_{13} and X_{14} correction paths.

Some groups are using coherent dedispersion (Hankins 1974) for their timing applications. The coherent dedispersion can be done before the application of the correlation-based RFI cancelling. If signals from the reference antenna were also coherently dedispersed in the same way, the technique we put forward will still effectively suppress interference. To first order, the dispersion has a similar form to a delay error, producing a near-linear phase drift with frequency; for broader bandwidths, the quadratic dependence would become important.

10. Conclusion

RFI subtraction can take place using cross power spectra between the astronomy data channels and RFI "reference" channels. In principle, the reference channel can also be an astronomy channel provide it carries an astronomy signal that is uncorrelated with the astronomy in the channel that is being corrected.

Improved results would be expected from a system with higher digitization precision. In addition, more attention should be given to standard astronomical calibration procedures at the time of data acquisition; spectral passband calibration, for example, is necessary in order to make a fair test of RFI subtraction in a real application. A clear refinement will be to implement this scheme using two reference antennas that are spatially separated (as in Fig 1) in order to avoid correlated noise contributions, while still obtaining as clear and stable path to the RFI source as possible. The cross power spectra from the two spatially separated antennas would form an optimal RFI reference spectrum C_{34} for use in the Eqns 12-14. To avoid problems with differential delay causing loss of coherence in the reference signal, the spectrometer would need to operate with spectral resolution $\Delta f = (\Delta\phi/2\pi)c/L << c/L$ where $\Delta\phi$ is the allowable phase rotation across a spectrometer channel and L is the spatial separation of the sensors. The 2.4 kHz spectrometer resolution emulated in software for the study reported here would allow spatial separations of up to 1200m, if $\Delta\phi$ is required to be less than 0.02π radians.

The case of multiple interferers and time variability of the RFI $H(t)$ impulse responses will require a greater number of sensors and correlator capacity devoted to processing the the RFI signals, as laid out in the analyses of Sault (1997) and Ellingson (1999) .

Scattered solar radiation could be treated similarly but with the important difference that the Sun generates a dual polarized signal with a variable polarized component; this will necessitate a processing path more akin to the sub-space decomposition (Ellingson 1999; Lesham et al. 2000), in order to identify orthogonal components of the solar "rfi" signals.

The authors are grateful to W. van Stratten, M. Bailes, S. Anderson, S. Ellingson, R. Sault, R. Ekers, J. Bunton, L. Kewley and M. Smith for helpful comments and discussion. F.B. is grateful to the ATNF in Epping, NSW, the Department of Astronomy at OSU, Columbus, OH, and to the IAS, Princeton, NJ for their hospitality while this work was done.

REFERENCES

Australian_Communications_Authority 1998, Communications Legislation

Barnbaum, C. & Bradley, R. 1998, Astron. J., 115, 2598

Bell, J. F. et al. 2000, Proc. Astr. Soc. Aust. submitted

Ekers, R. D. & Bell, J. F. 2000, in The Universe at Low Radio Frequencies, IAU Symposium 199, Pune, Dec. 1999., (San Francisco: PASP), in press

Ellingson, S. W. 1999, in The Elizabeth and Frederick White Conference on Radio Frequency Interference Mitigation Strategies, Sydney, Dec. 1999, ed. J. F. Bell & L. Kewley, (http://www.atnf.csiro.au/SKA/intmit/atnf/conf/: CSIRO ATNF)

Ellingson, S. W., Bunton, J. D., & Bell, J. F. 2000, in Astronomical Telescopes and Instrumentation 2000 - Radio Telescopes, SPIE conference 4015, SPIE, in press

Ellingson, S. W. & Hampson, G. A. 2000, IEEE transactions on Antennas and Propgation. submitted

Hampson, G. A., Goris, M., Joseph, A., & Smits, F. 1998, in IEEE Digital Signal Processing Workshop - Bryce Canyon USA, IEEE

Hankins, T. H. 1974, A&AS, 15, 363+

Kewley, L., Sault, R. J., Bell, J. F., Gray, D., Kestevan, M. J., & Ekers, R. D. 2000. in prep

Kewley, L., Sault, R. J., & Ekers, R. D. 1999, in The Elizabeth and Frederick White Conference on Radio Frequency Interference Mitigation Strategies, Sydney, Dec. 1999, ed. J. F. Bell & L. Kewley, (http://www.atnf.csiro.au/SKA/intmit/atnf/conf/: CSIRO ATNF)

Lesham, A. & van der Veen, A. J. 1999a, in IEEE workshop on Signal Processing Advances in Wireless Communications, IEEE

Lesham, A. & van der Veen, A. J. 1999b, in Proc. IEEE workshop on Higher Order Statistics, IEEE

Lesham, A., van der Veen, A. J., & Boonstra, A. J. 2000, Astrophys. J. in press

Sarkissian, J. M. 1999, in The Elizabeth and Frederick White Conference on Radio Frequency Interference Mitigation Strategies, Sydney, Dec. 1999, ed. J. F. Bell & L. Kewley, (http://www.atnf.csiro.au/SKA/intmit/atnf/conf/: CSIRO ATNF)

Sault, R. J. 1997, in 1kT Technical Workshop, Sydney, Dec. 1997, ed. W. Brouw, (http://www.atnf.csiro.au/SKA/WS: CSIRO ATNF)

Smolders, B. & Hampson, G. A. 2000, IEEE transactions on Antennas and Propgation. submitted

Staveley-Smith, L. et al. 1996, Proc. Astr. Soc. Aust., 13, 243

van Straten, W., Britton, M. C., Bailes, M., Anderson, S. B., & Kulkarni, S. 2000, in Pulsar Astronomy - 2000 and Beyond, ed. M. Kramer, N. Wex, & R. Wielebinski, (San Franciso: PASP), in press

This 2-column preprint was prepared with the AAS LaTeX macros v5.0.